

Research Article

A New Type-3 Fuzzy PID for Energy Management in Microgrids

Weiping Fan ¹, Ardashir Mohammadzadeh ², Nasreen Kausar ^{3,4}, Dragan Pamucar ⁵,
and Nasr Al Din Ide ⁶

¹Swan College, Central South University of Forestry and Technology, Changsha, 410210 Hunan, China

²Multidisciplinary Center for Infrastructure Engineering, Shenyang University of Technology, Shenyang 110870, China

³Department of Mathematics and Statistics, Quaid e Azam university, Islamabad, Pakistan

⁴Department of Mathematics, Faculty of Arts and Sciences, Yildiz Technical University, Esenler, 34210 Istanbul, Turkey

⁵Faculty of Organizational Sciences, University of Belgrade, Belgrade, Serbia

⁶Department of Mathematics, University of Aleppo, Aleppo, Syria

Correspondence should be addressed to Nasr Al Din Ide; ide1112002@yahoo.ca

Received 3 June 2022; Accepted 4 July 2022; Published 29 July 2022

Academic Editor: S. E. Najafi

Copyright © 2022 Weiping Fan et al. This is an open access article distributed under the Creative Commons Attribution License, which permits unrestricted use, distribution, and reproduction in any medium, provided the original work is properly cited.

More recently, type-3 (T3) fuzzy logic systems (FLSs) with better learning ability and uncertainty modeling have been presented. On other hand, the proportional-integral-derivative (PID) is commonly employed in most industrial control systems, because of its simplicity and efficiency. The measurement errors, nonlinearities, and uncertainties degrade the performance of conventional PIDs. In this study, for the first time, a new T3-FLS-based PID scheme with deep learning approach is introduced. In addition to rules, the parameters of fuzzy sets are also tuned such that a fast regulation efficiency is obtained. Unlike the most conventional approaches, the suggested tuning approach is done in an online scheme. Also, a nonsingleton fuzzification is suggested to reduce the effect of sensor errors. The proposed scheme is examined on a case-study microgrid (MG), and its good frequency stabilization performance is demonstrated in various hard conditions such as variable load, unknown dynamics, and variation in renewable energy (RE) sources.

1. Introduction

Today, as technology advances and the consumerist population grows, providing sustainable, safe, and clean energy is one of the human's core concerns. Regarding limitation of non-RE resources and the environmental problems caused by their consumption, different countries have decided to choose other energy sources, including renewable sources, as a future and sustainable energy source. Although RE sources are available worldwide, many of these sources are not available seven days a week, 24 hours a day. Some days may be windier than others, the sun does not shine at night, and droughts may occur for a period of time. It can be unpredictable weather events that disrupt these technologies. To improve the sustainability, some energy storage systems and modern controllers should be used to make a balance between consumption and germination [1, 2].

Because of its simplicity and capacity, PID control systems are extensively employed in most industrial problems such as mechanical engineering, chaotic systems, and electrical engineering [3]. In proportional control mode of PID, the output is proportional to the amount of error (hence, it is called proportional). If the error is large, the controller output is large, and if the error is small, the controller output is small. The adjustable parameter of proportional control is called controller gain. The higher the controller gain leads to the higher the proportional error. If the gain is adjusted too high, the control loop will start to oscillate and become unstable [4]. On the other hand, if the gain is too low, responding to disturbances or changes in the setpoint will not be effective enough. There is one major drawback to using a proportional controller alone, and that is offset. Offset is a persistent error that cannot be eliminated by proportional control alone. The integrated control mode continuously

increases or decreases the controller output to minimize error. By the larger error, the integral mode increases or decreases the output rapidly, and by the smaller error, changes will be occur more slowly. The output of the derivative controller is directly related to the error rate over time. Derivative controllers are generally used when process variables start to fluctuate or change at very high speeds. Derivative controllers are also used to predict the future performance of the error by means of an error curve. In this mode, when the error changes are large, the derivative mode will produce more control action. When the error does not change, the derivative operation will be zero. When the derivative time is too long, fluctuations occur in this mode and the closed loop becomes unstable. Then, in real-world applications, the PID parameters should be carefully tuned [5–7].

2. Literature Review

The main approach that has been frequently used for PID tuning is the use of evolutionary based methods. For example, the fractional PID is investigated in [8], and by the use of grasshopper optimization algorithm, the parameters of PID are tuned. In [9], a predictive controller is used to improve the performance of PI controller. In [10], a regulator is constructed using a reinforcement method, and it is evaluated on an isolated MG. The developed genetic algorithm (GA) by the use of nondominated sorting approach is suggested in [11], to design a frequency regulator. The application of FLSs in designing of voltage controller is studied in [12]. The particle swarm optimization (PSO) is used in [13] for optimization, and it is examined on an inverter-based MG. In [14], the various approaches are reviewed.

One of main approaches to tune the PIDs is the use of FLSs and neural networks [15, 16]. The FLSs are widely used for approximation problems [17, 18]. For example, in [19], a PID is designed using type-1 FLSs, and it is applied for temperature control. In [20], a defuzzification is suggested for FLSs to decrease the computations, and then, a PID is designed based on the simplified FLS. The backstepping PID is studied in [21], and a FLS is formulated to estimate the uncertainties. Similar to classical PIDs that are reviewed in the above paragraph, some evolutionary-based algorithms have also been developed for tuning of FLS-PIDs. In these methods, the evolutionary-based techniques are used to tune FLS rules, and the output of FLSs determines the gains of PID [22]. In [23], a fractional-order version of PID is designed, and one FLS is used to optimize all gains. In [24], the frequency control in MG is studied, and a FLS-based PID is schemed. In [25], the efficiency of FLS-PID is examined on a power system, and the accuracy improvement by FLSs is shown. A comparative study in [26] shows that FLSs well amend the accuracy of PIDs in versus of disturbances and uncertainties.

The type-2 FLSs have been rarely used in MG. For example, in [27], a deep-learned T2-FLS-based control technique is developed, and the good efficiency of T2-FLSs is verified. In [28], a T2-FLS is formulated for optimizing a PID, and its performance is examined by a stabilization problem in MGs. In [29], the membership functions of a generalized

IT2FS are optimized, and a controller is designed for both frequency and voltage management. The equilibrium optimization scheme is used in [30] for tuning the parameters of PID controller on the basis of T2-FLSs. In [31], a type-2 PID is developed, and its efficiency is compared by applying on MG. In [32], the efficiency of the T2-FLS-based control systems is evaluated on the basis of Harris approach. A PID is developed in [33] using T2-FLSs, and it is demonstrated that high-order FLSs enhance the accuracy.

More recently, it has been shown that high-order FLSs such as type-3 FLSs and generalized FLSs give better efficiency in real-world engineering problems. For example, in [34], a T3-FLS is used for energy management, and by various comparisons, the superiority of T3-FLSs is shown. In [35], a T3-FLS-based controller is designed for MGs and the fluctuation of solar energies is tackled by the use of T3-FLSs. The capability of T3-FLSs in a real-world 5G telecom application is tested in [36], and it is verified that T3-FLSs result in better stabilization efficiency. Similarly, in [37], the better estimation efficiency and stabilization performance of T3-FLSs are examined in an experimental DC power system.

3. Motivations

The literature review shows that in most of PID tuning approaches, trial-and-error methods and some evolutionary algorithms are commonly used. However, the uncertainties, nonlinearities, and changes in dynamic parameters decrease the performance of conventional approaches. Also, the evolutionary-based approaches are not suitable for practical systems, due to the high computational process of these algorithms. Furthermore, in most of investigated methods, the tuning is done in an off-line schedule, and then, the unpredictable online disturbances are not supported. Although some FLS-based PIDs have been presented, most of the conventional FLSs are vulnerable to the plant's uncertainties, sensor errors, and nonlinearities.

4. Novelettes

The basic advantages of the designed regulator are as follows:

- (i) A type-3 FLS-based PID with higher capability and using fractional-order calculus is introduced
- (ii) There is no need for MG dynamics
- (iii) Unlike most FLS-based PIDs, the structure of the suggested approach is nonlinear
- (iv) In addition to rules, the MFs are also tuned to speed up the learning
- (v) The tuning is done in an online approach, and the suggested PID is updated, at each sample time
- (vi) All gains are tuned simultaneously
- (vii) Nonsingleton fuzzification decreases the effect of sensor error

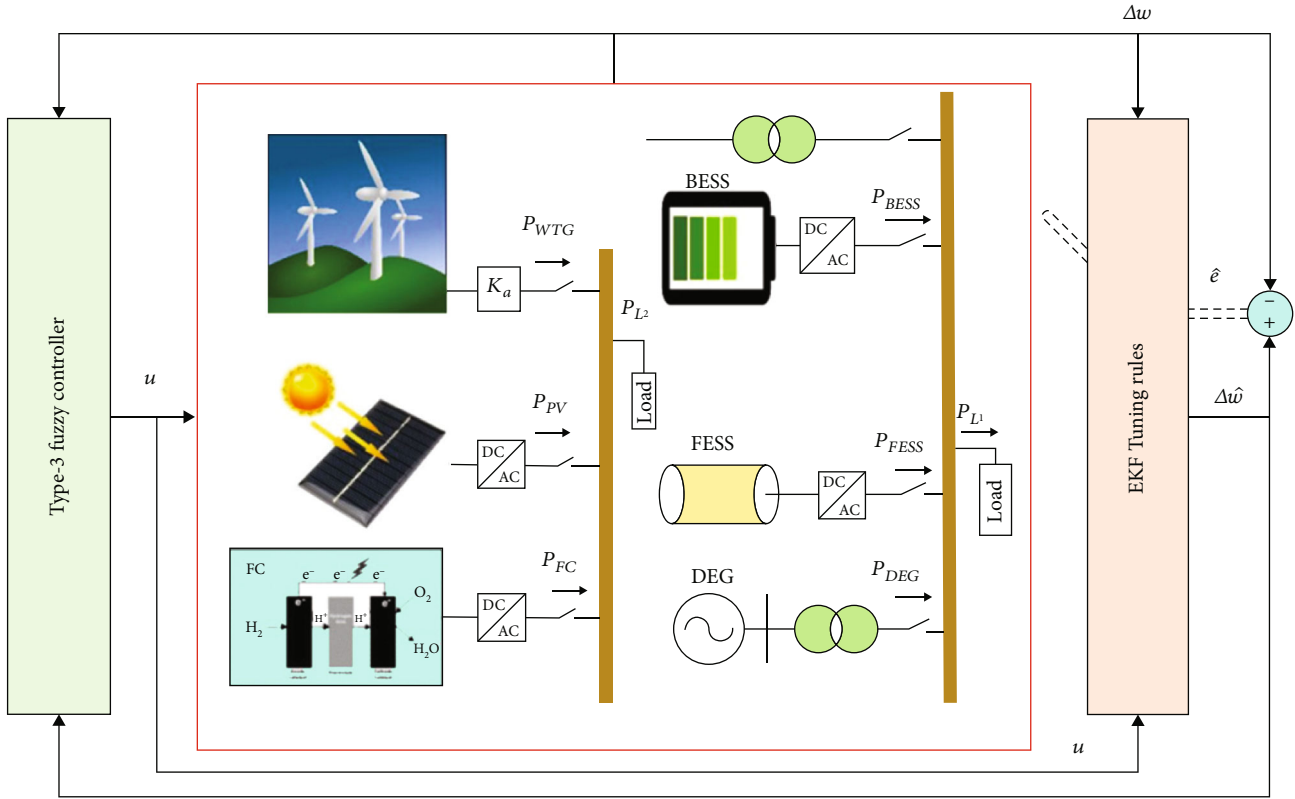


FIGURE 1: General diagram.

- (viii) In various hard conditions, such as considering load changes, variation of wind/solar powers, and dynamic disturbances, the better efficiency of the suggested approach is demonstrated

5. Problem Formulation

Power imbalance is felt by its effect on the speed or frequency of the generator. If the load is reduced and the output is increased, the generator tends to enhance its speed/frequency. By increasing load and production shortage, the speed/frequency of the generator decreases. The variation of frequency from its nominal value is chosen as a signal to excite the automatic controller. Then, a power balance at a constant frequency is an important problem [38, 39].

The load frequency control (LFC) loop responds only to small amplitude and slow load and frequency changes and is unable to control in emergencies and the resulting power imbalance. System control in emergencies and sudden changes is examined by studying the transient stability and protection of systems.

A general view is shown in Figure 1. The designed control scheme does not use the mathematical models. The suggested control technique is well optimized and tackles the effect of perturbations such as variation of weather conditions and output lead.

The main purposes of LFC are as follows: maintaining the frequency uniformly, dividing the system load between the generators optimally and preferably economically, and regulating the power exchanged from the communication

lines in the planned values. In fact, the change in the frequency of the system and the actual power of the communication lines must be eliminated by changing the output.

6. Fuzzy PID Controller

PIDs are commonly employed in most industrial control systems because of their simplicity and capacity. The control performance of conventional PIDs degrades under nonlinearities, uncertainties, and parameter changes. In the conventional FLS-based PIDs, FLSs are used to alter the PID gains. The closed-loop error and its derivative are commonly used as inputs of FLSs. The output of FLS determines the gains of PIDs. In the suggested approach, the output of designed type-3 FLS directly determines the output. The input variables are error and its fractional derivative and integral. Rules of FLS are tuned such that an error-based cost function is minimized. The general scheme is shown in Figure 2.

7. Type-3 FLS

The type-3 FLS [40] is a more capable version of the type-2 FLS. Figure 3 depicts a broad overview of the hypothesized T3-FLS. In T3-FLSs, secondary membership function (MF) is likewise a type-2 MF, as illustrated in Figure 4. In contrast to conventional MFs, the top/lower boundaries of memberships are not constant. Because of these characteristics, type-3 MFs can manage a higher amount of uncertainty. The computations are discussed in this section:

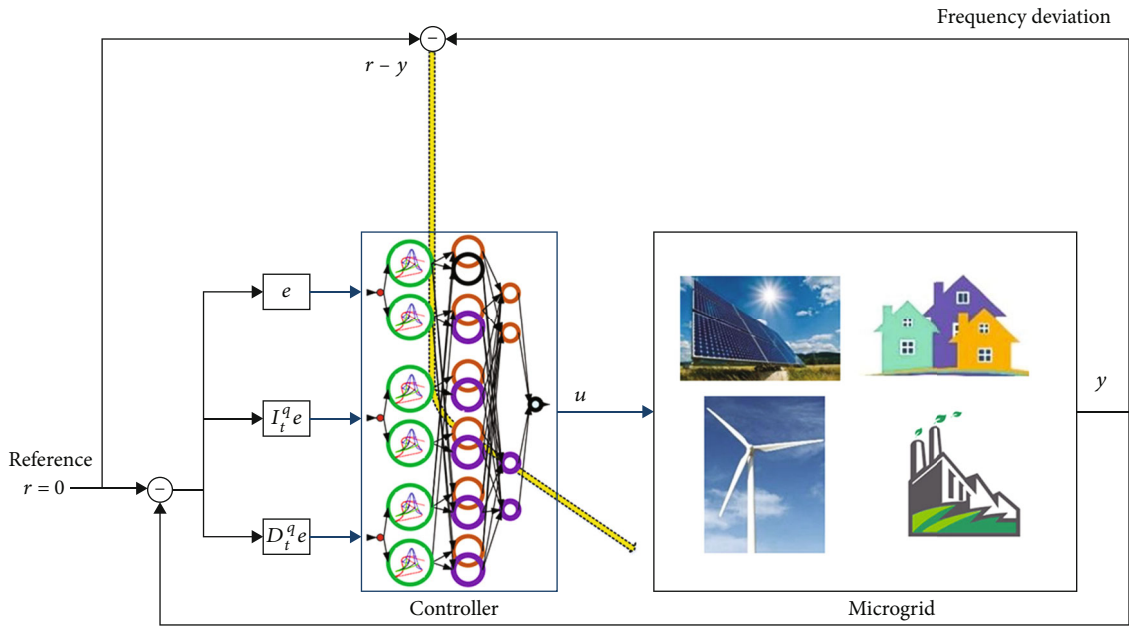


FIGURE 2: General view.

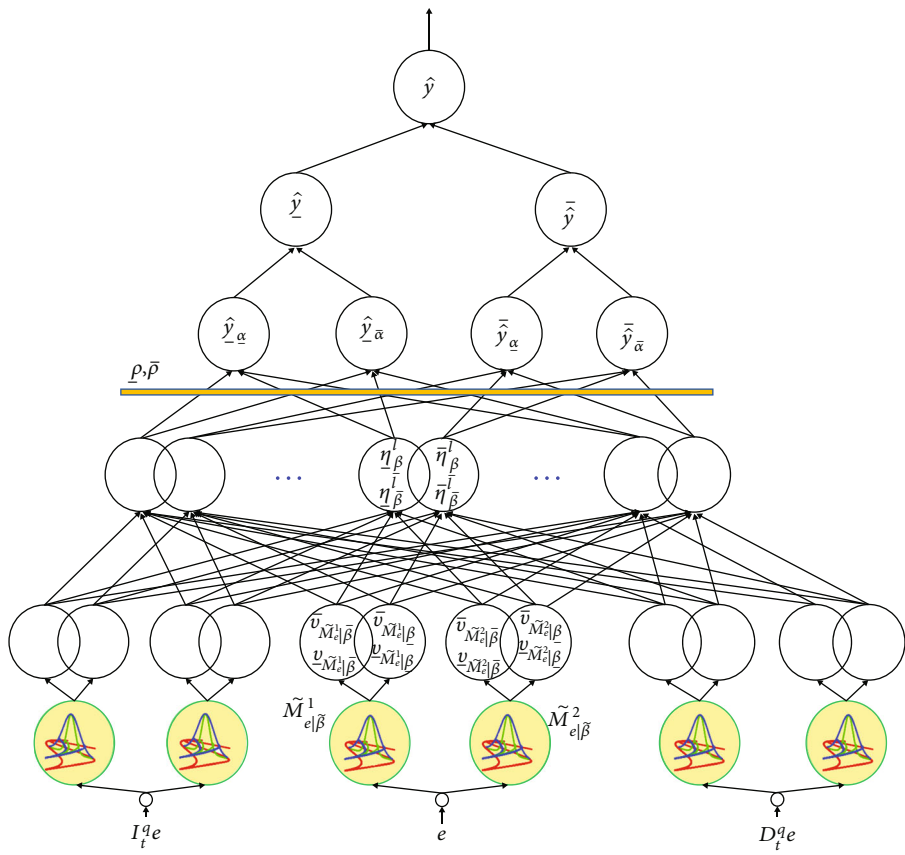


FIGURE 3: A general view on T3-FLS.

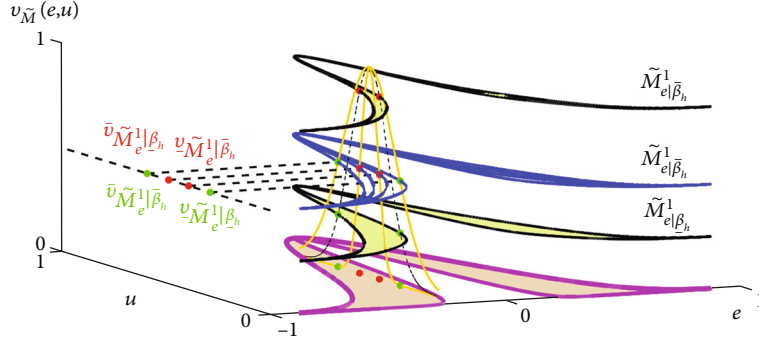


FIGURE 4: Type-3 MF.

(1) The input variables are e , $I_t^q e$, and $D_t^q e$, where

$$D_t^q e(t) = \frac{\int_0^t (e(x)/(t-x)^q) dx}{\Gamma(1-q)},$$

$$I_t^q e(t) = \frac{\int_0^t (t-x)^{q-1} e(x) dx}{\Gamma(q)}$$
(1)

(2) For inputs e , $I_t^q e$, and $D_t^q e$, MFs are considered as \tilde{M}_e^1 , \tilde{M}_e^2 , $M_{I_t^q e}^1 - \tilde{M}_{I_t^q e}^2$, and $M_{D_t^q e}^1 - \tilde{M}_{D_t^q e}^2$, respectively. As illustrated in Figure 4, each MF is horizontally split into n levels. The memberships for horizontal slice level β_h are calculated for each input, as illustrated in Figure 4. A Gaussian MF is considered for inputs to handle the sensor errors. The upper/lower memberships at level β_h for input e are calculated as follows:

$$\bar{v}_{\tilde{M}_e^j | \beta_h} = \exp \left(- \frac{\left(\bar{e}_{\beta_h} - c_{\tilde{M}_e^j | \beta_h} \right)^2}{\bar{\vartheta}_{\tilde{M}_e^j | \beta_h}^2} \right),$$

$$\bar{v}_{\tilde{M}_e^j | \underline{\beta}_h} = \exp \left(- \frac{\left(\bar{e}_{\underline{\beta}_h} - c_{\tilde{M}_e^j | \underline{\beta}_h} \right)^2}{\bar{\vartheta}_{\tilde{M}_e^j | \underline{\beta}_h}^2} \right),$$

$$\underline{v}_{\tilde{M}_e^j | \bar{\beta}_h} = \exp \left(- \frac{\left(\underline{e}_{\bar{\beta}_h} - c_{\tilde{M}_e^j | \bar{\beta}_h} \right)^2}{\underline{\vartheta}_{\tilde{M}_e^j | \bar{\beta}_h}^2} \right),$$

$$\underline{v}_{\tilde{M}_e^j | \underline{\beta}_h} = \exp \left(- \frac{\left(\underline{e}_{\underline{\beta}_h} - c_{\tilde{M}_e^j | \underline{\beta}_h} \right)^2}{\underline{\vartheta}_{\tilde{M}_e^j | \underline{\beta}_h}^2} \right),$$
(2)

where

$$\bar{e}_{\beta_h} = \frac{e \bar{\vartheta}_{\tilde{M}_e^j | \beta_h}^2 + \sigma_s^2 c_{\tilde{M}_e^j | \beta_h}}{\bar{\vartheta}_{\tilde{M}_e^j | \beta_h}^2 + \sigma_s^2},$$

$$\bar{e}_{\underline{\beta}_h} = \frac{e \bar{\vartheta}_{\tilde{M}_e^j | \underline{\beta}_h}^2 + \sigma_s^2 c_{\tilde{M}_e^j | \underline{\beta}_h}}{\bar{\vartheta}_{\tilde{M}_e^j | \underline{\beta}_h}^2 + \sigma_s^2},$$

$$\underline{e}_{\bar{\beta}_h} = \frac{e \underline{\vartheta}_{\tilde{M}_e^j | \bar{\beta}_h}^2 + \sigma_s^2 c_{\tilde{M}_e^j | \bar{\beta}_h}}{\underline{\vartheta}_{\tilde{M}_e^j | \bar{\beta}_h}^2 + \sigma_s^2},$$

$$\underline{e}_{\underline{\beta}_h} = \frac{e \underline{\vartheta}_{\tilde{M}_e^j | \underline{\beta}_h}^2 + \sigma_s^2 c_{\tilde{M}_e^j | \underline{\beta}_h}}{\underline{\vartheta}_{\tilde{M}_e^j | \underline{\beta}_h}^2 + \sigma_s^2},$$

(3)

where, $h = 1, \dots, n$, $j = 1, 2$, $c_{\tilde{M}_e^j | \beta_h}$ is the center of MF $\tilde{M}_e^j | \beta_h$, and $\bar{\vartheta}_{\tilde{M}_e^j | \beta_h}$ and $\underline{\vartheta}_{\tilde{M}_e^j | \beta_h}$ are the upper/lower standard-divisions (SD) for $\tilde{M}_e^j | \beta_h$. For input $I_t^q e$, we have

$$\bar{v}_{\tilde{M}_{I_t^q e}^j | \beta_h} = \exp \left(- \frac{\left(I_t^q \bar{e}_{\beta_h} - c_{\tilde{M}_{I_t^q e}^j | \beta_h} \right)^2}{\bar{\vartheta}_{\tilde{M}_{I_t^q e}^j | \beta_h}^2} \right),$$

$$\bar{v}_{\tilde{M}_{I_t^q e}^j | \underline{\beta}_h} = \exp \left(- \frac{\left(I_t^q \bar{e}_{\underline{\beta}_h} - c_{\tilde{M}_{I_t^q e}^j | \underline{\beta}_h} \right)^2}{\bar{\vartheta}_{\tilde{M}_{I_t^q e}^j | \underline{\beta}_h}^2} \right),$$

$$\underline{v}_{\tilde{M}_{I_t^q e}^j | \bar{\beta}_h} = \exp \left(- \frac{\left(I_t^q \underline{e}_{\bar{\beta}_h} - c_{\tilde{M}_{I_t^q e}^j | \bar{\beta}_h} \right)^2}{\underline{\vartheta}_{\tilde{M}_{I_t^q e}^j | \bar{\beta}_h}^2} \right),$$

$$\underline{v}_{\tilde{M}_{I_t^q e}^j | \underline{\beta}_h} = \exp \left(- \frac{\left(I_t^q \underline{e}_{\underline{\beta}_h} - c_{\tilde{M}_{I_t^q e}^j | \underline{\beta}_h} \right)^2}{\underline{\vartheta}_{\tilde{M}_{I_t^q e}^j | \underline{\beta}_h}^2} \right),$$

$$\underline{v}_{\tilde{M}_{I_t^q e}^j | \beta_h} = \exp \left(- \frac{\left(I_t^q \underline{e}_{\beta_h} - c_{\tilde{M}_{I_t^q e}^j | \beta_h} \right)^2}{\underline{\vartheta}_{\tilde{M}_{I_t^q e}^j | \beta_h}^2} \right),$$
(4)

where

$$\begin{aligned}
I_t^q \bar{e}_{\bar{\beta}_h} &= \frac{I_t^q e^{\bar{\vartheta}_{\bar{M}_c^j|\bar{\beta}_h}^2} + \sigma_s^2 c_{\bar{M}_c^j|\bar{\beta}_h}}{\bar{\vartheta}_{\bar{M}_c^j|\bar{\beta}_h}^2 + \sigma_s^2}, \\
I_t^q \bar{e}_{\underline{\beta}_h} &= \frac{I_t^q e^{\bar{\vartheta}_{\bar{M}_c^j|\underline{\beta}_h}^2} + \sigma_s^2 c_{\bar{M}_c^j|\underline{\beta}_h}}{\bar{\vartheta}_{\bar{M}_c^j|\underline{\beta}_h}^2 + \sigma_s^2}, \\
I_t^q \underline{e}_{\bar{\beta}_h} &= \frac{I_t^q e^{\underline{\vartheta}_{\bar{M}_c^j|\bar{\beta}_h}^2} + \sigma_s^2 c_{\bar{M}_c^j|\bar{\beta}_h}}{\underline{\vartheta}_{\bar{M}_c^j|\bar{\beta}_h}^2 + \sigma_s^2}, \\
I_t^q \underline{e}_{\underline{\beta}_h} &= \frac{I_t^q e^{\underline{\vartheta}_{\bar{M}_c^j|\underline{\beta}_h}^2} + \sigma_s^2 c_{\bar{M}_c^j|\underline{\beta}_h}}{\underline{\vartheta}_{\bar{M}_c^j|\underline{\beta}_h}^2 + \sigma_s^2},
\end{aligned} \tag{5}$$

where $h = 1, \dots, n$, $j = 1, 2$, $c_{\bar{M}_{I_t^q e}^j|\bar{\beta}_h}$ denotes center of $\bar{M}_{I_t^q e}^j|\bar{\beta}_h$, and $\bar{\vartheta}_{\bar{M}_{I_t^q e}^j|\bar{\beta}_h}$ and $\underline{\vartheta}_{\bar{M}_{I_t^q e}^j|\bar{\beta}_h}$ are the upper/lower SD for $\bar{M}_{I_t^q e}^j|\bar{\beta}_h$. Similarly, for $D_t^q e$, we have

$$\begin{aligned}
\bar{v}_{\bar{M}_{D_t^q e}^j|\bar{\beta}_h} &= \exp \left(- \frac{\left(D_t^q \bar{e}_{\bar{\beta}_h} - c_{\bar{M}_{D_t^q e}^j|\bar{\beta}_h} \right)^2}{\bar{\vartheta}_{\bar{M}_{D_t^q e}^j|\bar{\beta}_h}^2} \right), \\
\bar{v}_{\bar{M}_{D_t^q e}^j|\underline{\beta}_h} &= \exp \left(- \frac{\left(D_t^q \bar{e}_{\underline{\beta}_h} - c_{\bar{M}_{D_t^q e}^j|\underline{\beta}_h} \right)^2}{\bar{\vartheta}_{\bar{M}_{D_t^q e}^j|\underline{\beta}_h}^2} \right), \\
\underline{v}_{\bar{M}_{D_t^q e}^j|\bar{\beta}_h} &= \exp \left(- \frac{\left(D_t^q \underline{e}_{\bar{\beta}_h} - c_{\bar{M}_{D_t^q e}^j|\bar{\beta}_h} \right)^2}{\underline{\vartheta}_{\bar{M}_{D_t^q e}^j|\bar{\beta}_h}^2} \right), \\
\underline{v}_{\bar{M}_{D_t^q e}^j|\underline{\beta}_h} &= \exp \left(- \frac{\left(D_t^q \underline{e}_{\underline{\beta}_h} - c_{\bar{M}_{D_t^q e}^j|\underline{\beta}_h} \right)^2}{\underline{\vartheta}_{\bar{M}_{D_t^q e}^j|\underline{\beta}_h}^2} \right),
\end{aligned} \tag{6}$$

where

$$\begin{aligned}
D_t^q \bar{e}_{\bar{\beta}_h} &= \frac{I_t^q e^{\bar{\vartheta}_{\bar{M}_c^j|\bar{\beta}_h}^2} + \sigma_s^2 c_{\bar{M}_c^j|\bar{\beta}_h}}{\bar{\vartheta}_{\bar{M}_c^j|\bar{\beta}_h}^2 + \sigma_s^2}, \\
D_t^q \bar{e}_{\underline{\beta}_h} &= \frac{I_t^q e^{\bar{\vartheta}_{\bar{M}_c^j|\underline{\beta}_h}^2} + \sigma_s^2 c_{\bar{M}_c^j|\underline{\beta}_h}}{\bar{\vartheta}_{\bar{M}_c^j|\underline{\beta}_h}^2 + \sigma_s^2},
\end{aligned}$$

$$\begin{aligned}
D_t^q \underline{e}_{\bar{\beta}_h} &= \frac{D_t^q e^{\underline{\vartheta}_{\bar{M}_c^j|\bar{\beta}_h}^2} + \sigma_s^2 c_{\bar{M}_c^j|\bar{\beta}_h}}{\underline{\vartheta}_{\bar{M}_c^j|\bar{\beta}_h}^2 + \sigma_s^2}, \\
D_t^q \underline{e}_{\underline{\beta}_h} &= \frac{D_t^q e^{\underline{\vartheta}_{\bar{M}_c^j|\underline{\beta}_h}^2} + \sigma_s^2 c_{\bar{M}_c^j|\underline{\beta}_h}}{\underline{\vartheta}_{\bar{M}_c^j|\underline{\beta}_h}^2 + \sigma_s^2},
\end{aligned} \tag{7}$$

where $h = 1, \dots, n$, $j = 1, 2$, $c_{\bar{M}_{D_t^q e}^j|\bar{\beta}_h}$ denotes the center of $\bar{M}_{D_t^q e}^j|\bar{\beta}_h$, and $\bar{\vartheta}_{\bar{M}_{D_t^q e}^j|\bar{\beta}_h}$ and $\underline{\vartheta}_{\bar{M}_{D_t^q e}^j|\bar{\beta}_h}$ are the upper/lower SD for $\bar{M}_{D_t^q e}^j|\bar{\beta}_h$.

(3) The rule firing at $\bar{\beta}_h$ is obtained as

$$\begin{aligned}
\bar{\eta}_{\bar{\beta}_h}^1 &= \bar{v}_{\bar{M}_c^1|\bar{\beta}_h} \bar{v}_{\bar{M}_{I_t^q e}^1|\bar{\beta}_h} \bar{v}_{\bar{M}_{D_t^q e}^1|\bar{\beta}_h}, \\
\bar{\eta}_{\bar{\beta}_h}^2 &= \bar{v}_{\bar{M}_c^1|\bar{\beta}_h} \bar{v}_{\bar{M}_{I_t^q e}^1|\bar{\beta}_h} \bar{v}_{\bar{M}_{D_t^q e}^2|\bar{\beta}_h}, \\
\bar{\eta}_{\bar{\beta}_h}^3 &= \bar{v}_{\bar{M}_c^1|\bar{\beta}_h} \bar{v}_{\bar{M}_{I_t^q e}^2|\bar{\beta}_h} \bar{v}_{\bar{M}_{D_t^q e}^1|\bar{\beta}_h}, \\
\bar{\eta}_{\bar{\beta}_h}^4 &= \bar{v}_{\bar{M}_c^1|\bar{\beta}_h} \bar{v}_{\bar{M}_{I_t^q e}^2|\bar{\beta}_h} \bar{v}_{\bar{M}_{D_t^q e}^2|\bar{\beta}_h}, \\
\bar{\eta}_{\bar{\beta}_h}^5 &= \bar{v}_{\bar{M}_c^2|\bar{\beta}_h} \bar{v}_{\bar{M}_{I_t^q e}^1|\bar{\beta}_h} \bar{v}_{\bar{M}_{D_t^q e}^1|\bar{\beta}_h}, \\
\bar{\eta}_{\bar{\beta}_h}^6 &= \bar{v}_{\bar{M}_c^2|\bar{\beta}_h} \bar{v}_{\bar{M}_{I_t^q e}^1|\bar{\beta}_h} \bar{v}_{\bar{M}_{D_t^q e}^2|\bar{\beta}_h}, \\
\bar{\eta}_{\bar{\beta}_h}^7 &= \bar{v}_{\bar{M}_c^2|\bar{\beta}_h} \bar{v}_{\bar{M}_{I_t^q e}^2|\bar{\beta}_h} \bar{v}_{\bar{M}_{D_t^q e}^1|\bar{\beta}_h}, \\
\bar{\eta}_{\bar{\beta}_h}^8 &= \bar{v}_{\bar{M}_c^2|\bar{\beta}_h} \bar{v}_{\bar{M}_{I_t^q e}^2|\bar{\beta}_h} \bar{v}_{\bar{M}_{D_t^q e}^2|\bar{\beta}_h}
\end{aligned} \tag{8}$$

For $\underline{\beta}_h$, we have

$$\begin{aligned}
\bar{\eta}_{\underline{\beta}_h}^1 &= \bar{v}_{\bar{M}_c^1|\underline{\beta}_h} \bar{v}_{\bar{M}_{I_t^q e}^1|\underline{\beta}_h} \bar{v}_{\bar{M}_{D_t^q e}^1|\underline{\beta}_h}, \\
\bar{\eta}_{\underline{\beta}_h}^2 &= \bar{v}_{\bar{M}_c^1|\underline{\beta}_h} \bar{v}_{\bar{M}_{I_t^q e}^1|\underline{\beta}_h} \bar{v}_{\bar{M}_{D_t^q e}^2|\underline{\beta}_h}, \\
\bar{\eta}_{\underline{\beta}_h}^3 &= \bar{v}_{\bar{M}_c^1|\underline{\beta}_h} \bar{v}_{\bar{M}_{I_t^q e}^2|\underline{\beta}_h} \bar{v}_{\bar{M}_{D_t^q e}^1|\underline{\beta}_h}, \\
\bar{\eta}_{\underline{\beta}_h}^4 &= \bar{v}_{\bar{M}_c^1|\underline{\beta}_h} \bar{v}_{\bar{M}_{I_t^q e}^2|\underline{\beta}_h} \bar{v}_{\bar{M}_{D_t^q e}^2|\underline{\beta}_h}, \\
\bar{\eta}_{\underline{\beta}_h}^5 &= \bar{v}_{\bar{M}_c^2|\underline{\beta}_h} \bar{v}_{\bar{M}_{I_t^q e}^1|\underline{\beta}_h} \bar{v}_{\bar{M}_{D_t^q e}^1|\underline{\beta}_h}, \\
\bar{\eta}_{\underline{\beta}_h}^6 &= \bar{v}_{\bar{M}_c^2|\underline{\beta}_h} \bar{v}_{\bar{M}_{I_t^q e}^1|\underline{\beta}_h} \bar{v}_{\bar{M}_{D_t^q e}^2|\underline{\beta}_h}, \\
\bar{\eta}_{\underline{\beta}_h}^7 &= \bar{v}_{\bar{M}_c^2|\underline{\beta}_h} \bar{v}_{\bar{M}_{I_t^q e}^2|\underline{\beta}_h} \bar{v}_{\bar{M}_{D_t^q e}^1|\underline{\beta}_h}, \\
\bar{\eta}_{\underline{\beta}_h}^8 &= \bar{v}_{\bar{M}_c^2|\underline{\beta}_h} \bar{v}_{\bar{M}_{I_t^q e}^2|\underline{\beta}_h} \bar{v}_{\bar{M}_{D_t^q e}^2|\underline{\beta}_h}
\end{aligned} \tag{9}$$

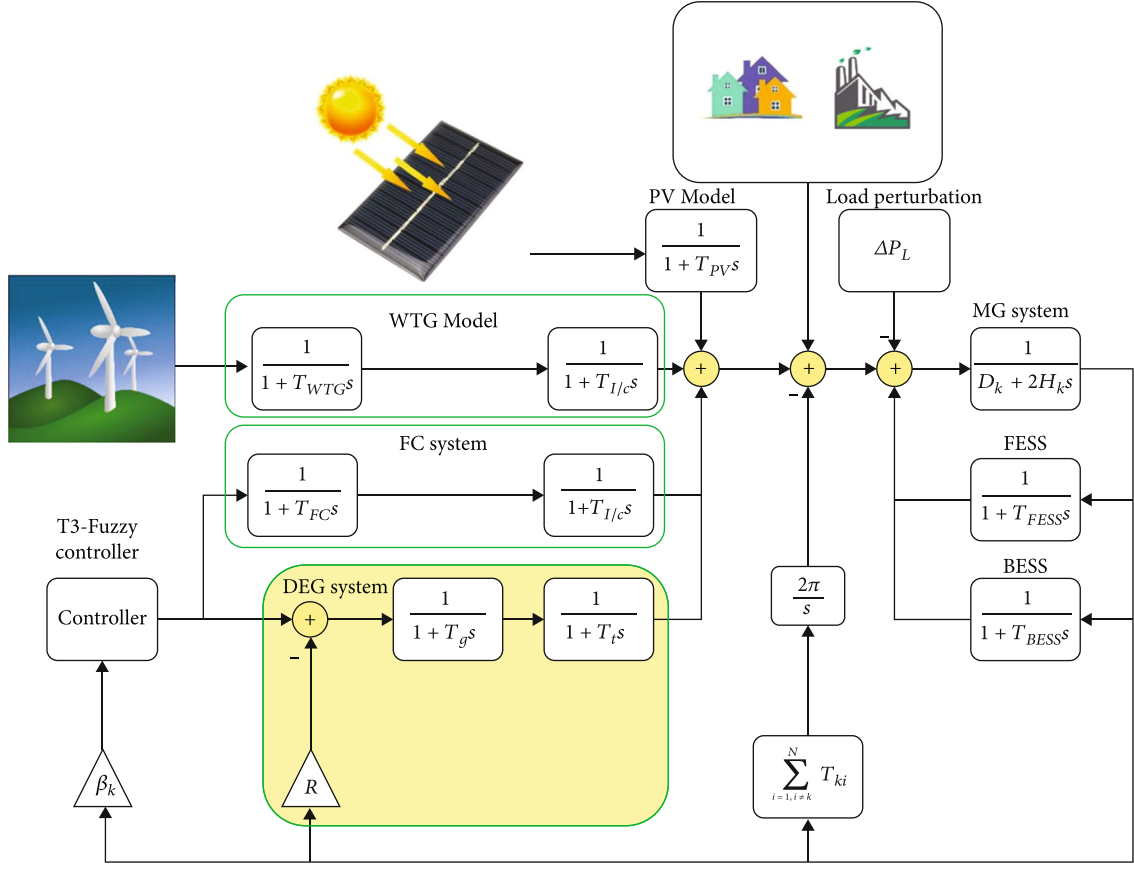


FIGURE 5: Case-study MG.

The lower firing degree of rules at upper/lower slice levels is obtained as

$$\underline{\eta}_{\beta_h}^1 = \bar{v}_{\tilde{M}_c^1} | \bar{\beta}_h \bar{v}_{\tilde{M}_{I/c}^1} | \bar{\beta}_h \bar{v}_{\tilde{M}_{D_i}^1} | \bar{\beta}_h ,$$

$$\underline{\eta}_{\beta_h}^2 = \bar{v}_{\tilde{M}_c^1} | \bar{\beta}_h \bar{v}_{\tilde{M}_{I/c}^1} | \bar{\beta}_h \bar{v}_{\tilde{M}_{D_i}^2} | \bar{\beta}_h ,$$

$$\underline{\eta}_{\beta_h}^3 = \bar{v}_{\tilde{M}_c^1} | \bar{\beta}_h \bar{v}_{\tilde{M}_{I/c}^2} | \bar{\beta}_h \bar{v}_{\tilde{M}_{D_i}^1} | \bar{\beta}_h ,$$

$$\underline{\eta}_{\beta_h}^4 = \bar{v}_{\tilde{M}_c^1} | \bar{\beta}_h \bar{v}_{\tilde{M}_{I/c}^2} | \bar{\beta}_h \bar{v}_{\tilde{M}_{D_i}^2} | \bar{\beta}_h ,$$

$$\underline{\eta}_{\beta_h}^5 = \bar{v}_{\tilde{M}_c^2} | \bar{\beta}_h \bar{v}_{\tilde{M}_{I/c}^1} | \bar{\beta}_h \bar{v}_{\tilde{M}_{D_i}^1} | \bar{\beta}_h ,$$

$$\underline{\eta}_{\beta_h}^6 = \bar{v}_{\tilde{M}_c^2} | \bar{\beta}_h \bar{v}_{\tilde{M}_{I/c}^1} | \bar{\beta}_h \bar{v}_{\tilde{M}_{D_i}^2} | \bar{\beta}_h ,$$

$$\underline{\eta}_{\beta_h}^7 = \bar{v}_{\tilde{M}_c^2} | \bar{\beta}_h \bar{v}_{\tilde{M}_{I/c}^2} | \bar{\beta}_h \bar{v}_{\tilde{M}_{D_i}^1} | \bar{\beta}_h ,$$

$$\underline{\eta}_{\beta_h}^8 = \bar{v}_{\tilde{M}_c^2} | \bar{\beta}_h \bar{v}_{\tilde{M}_{I/c}^2} | \bar{\beta}_h \bar{v}_{\tilde{M}_{D_i}^2} | \bar{\beta}_h ,$$

$$\underline{\eta}_{\beta_h}^1 = \bar{v}_{\tilde{M}_c^1} | \underline{\beta}_h \bar{v}_{\tilde{M}_{I/c}^1} | \underline{\beta}_h \bar{v}_{\tilde{M}_{D_i}^1} | \underline{\beta}_h ,$$

$$\underline{\eta}_{\beta_h}^2 = \bar{v}_{\tilde{M}_c^1} | \underline{\beta}_h \bar{v}_{\tilde{M}_{I/c}^1} | \underline{\beta}_h \bar{v}_{\tilde{M}_{D_i}^2} | \underline{\beta}_h ,$$

$$\underline{\eta}_{\beta_h}^3 = \bar{v}_{\tilde{M}_c^1} | \underline{\beta}_h \bar{v}_{\tilde{M}_{I/c}^2} | \underline{\beta}_h \bar{v}_{\tilde{M}_{D_i}^1} | \underline{\beta}_h ,$$

$$\underline{\eta}_{\beta_h}^4 = \bar{v}_{\tilde{M}_c^1} | \underline{\beta}_h \bar{v}_{\tilde{M}_{I/c}^2} | \underline{\beta}_h \bar{v}_{\tilde{M}_{D_i}^2} | \underline{\beta}_h ,$$

$$\underline{\eta}_{\beta_h}^5 = \bar{v}_{\tilde{M}_c^2} | \underline{\beta}_h \bar{v}_{\tilde{M}_{I/c}^1} | \underline{\beta}_h \bar{v}_{\tilde{M}_{D_i}^1} | \underline{\beta}_h ,$$

$$\underline{\eta}_{\beta_h}^6 = \bar{v}_{\tilde{M}_c^2} | \underline{\beta}_h \bar{v}_{\tilde{M}_{I/c}^1} | \underline{\beta}_h \bar{v}_{\tilde{M}_{D_i}^2} | \underline{\beta}_h ,$$

$$\underline{\eta}_{\beta_h}^7 = \bar{v}_{\tilde{M}_c^2} | \underline{\beta}_h \bar{v}_{\tilde{M}_{I/c}^2} | \underline{\beta}_h \bar{v}_{\tilde{M}_{D_i}^1} | \underline{\beta}_h ,$$

$$\underline{\eta}_{\beta_h}^8 = \bar{v}_{\tilde{M}_c^2} | \underline{\beta}_h \bar{v}_{\tilde{M}_{I/c}^2} | \underline{\beta}_h \bar{v}_{\tilde{M}_{D_i}^2} | \underline{\beta}_h .$$

TABLE 1: System parameter description (powers are in (KW)).

e_{BESS}	0.20 (s)	e_g	0.10 (s)	DEG	161	$I_i^q e_{L_2} =$ $I_i^q e_{L_1} =$
e_{PV}	1.84 (s)	e_{WTG}	1.44 (s)	PV	32	
H	0.18 (pu)	e_{FESS}	0.20 (s)	FC	71	
e_t	0.41 (s)	$e_{I/c}$	0.0035 (s)	FESS	47	220
e_{IN}	0.050 (s)	η_r	0.320 (pu/Hz)	BESS	45	

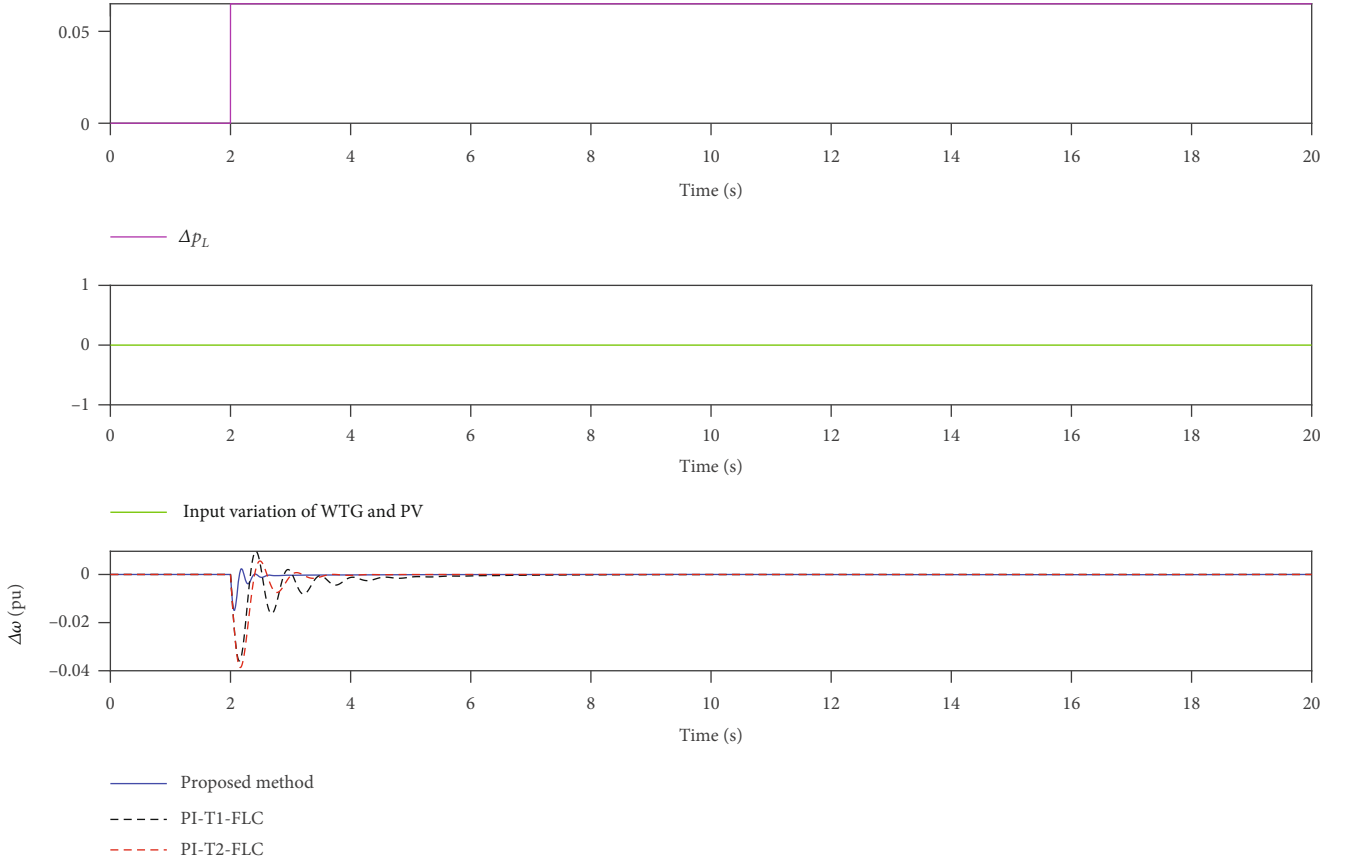


FIGURE 6: Scenario 1: load changes.

Considering the type reduction, the upper/lower bounds of control signal is computed as

$$\begin{aligned}
 \bar{y}_{\beta_h} &= \frac{\sum_{l=1}^{n_r} \bar{\eta}_{\beta_h}^l \bar{\rho}_l}{\sum_{l=1}^{n_r} (\bar{\eta}_{\beta_h}^l + \underline{\eta}_{\beta_h}^l)}, \\
 \bar{y}_{\underline{\beta}_h} &= \frac{\sum_{l=1}^{n_r} \bar{\eta}_{\underline{\beta}_h}^l \bar{\rho}_l}{\sum_{l=1}^{n_r} (\bar{\eta}_{\underline{\beta}_h}^l + \underline{\eta}_{\underline{\beta}_h}^l)}, \\
 \underline{y}_{\beta_h} &= \frac{\sum_{l=1}^{n_r} \underline{\eta}_{\beta_h}^l \underline{\rho}_l}{\sum_{l=1}^{n_r} (\bar{\eta}_{\beta_h}^l + \underline{\eta}_{\beta_h}^l)}, \\
 \underline{y}_{\underline{\beta}_h} &= \frac{\sum_{l=1}^{n_r} \underline{\eta}_{\underline{\beta}_h}^l \underline{\rho}_l}{\sum_{l=1}^{n_r} (\bar{\eta}_{\underline{\beta}_h}^l + \underline{\eta}_{\underline{\beta}_h}^l)},
 \end{aligned} \tag{11}$$

where n_r denotes the number of rules and $\underline{\rho}_l$ and $\bar{\rho}_l$ are the lower/upper of l th rule parameters.

The second type reduction is computed as

$$\begin{aligned}
 \bar{y} &= \frac{\sum_{h=1}^n \bar{\beta}_h \bar{y}_{\beta_h}}{\sum_{h=1}^n (\bar{\beta}_h + \underline{\beta}_h)} + \frac{\sum_{h=1}^n \underline{\beta}_h \bar{y}_{\underline{\beta}_h}}{\sum_{h=1}^n (\bar{\beta}_h + \underline{\beta}_h)}, \\
 \underline{y} &= \frac{\sum_{h=1}^n \bar{\beta}_h \underline{y}_{\beta_h}}{\sum_{h=1}^n (\bar{\beta}_h + \underline{\beta}_h)} + \frac{\sum_{h=1}^n \underline{\beta}_h \underline{y}_{\underline{\beta}_h}}{\sum_{h=1}^n (\bar{\beta}_h + \underline{\beta}_h)}.
 \end{aligned} \tag{12}$$

The output \hat{y} (control signal) is computed as

$$\hat{y} = \frac{\bar{y} + \underline{y}}{2}. \tag{13}$$

8. Learning Algorithm

The rule and MFs are tuned in this part.

8.1. Tuning of Rule Parameters. The EKF method tunes the rule parameters such that (14) is minimized:

$$J = \frac{1}{2} (\hat{y})^2, \tag{14}$$

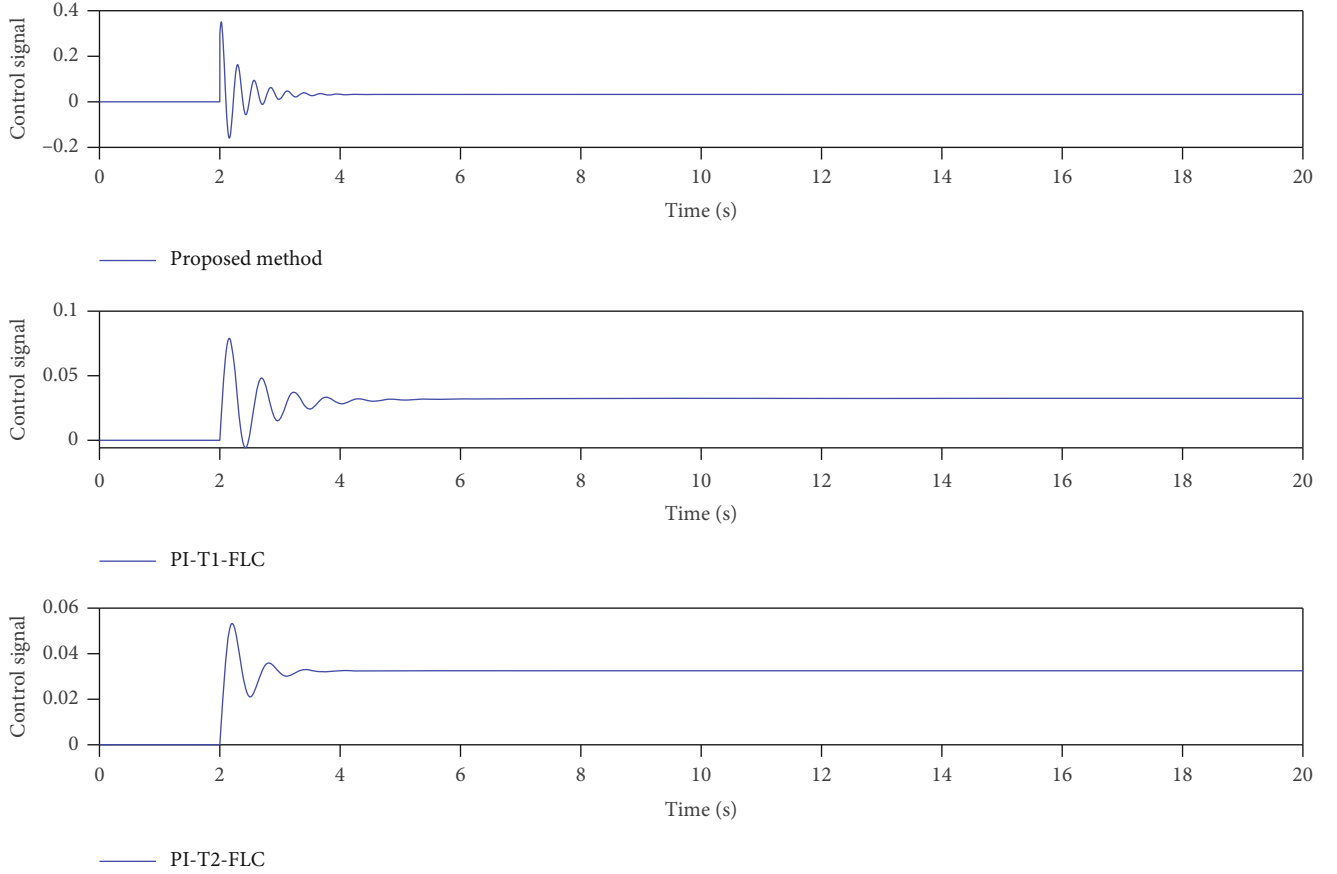


FIGURE 7: Scenario 1: control signals.

where \hat{y} is the output T3-FLS that denotes control signal. The adjusting laws for $\bar{\rho}$ and $\underline{\rho}$ are computed as

$$\begin{aligned}\bar{\rho}(t) &= \bar{\rho}(t-1) + \bar{\xi}(t)\bar{\chi}(t)(-\hat{y}), \\ \underline{\rho}(t) &= \underline{\rho}(t-1) + \underline{\xi}(t)\underline{\chi}(t)(-\hat{y}),\end{aligned}\quad (15)$$

where $\bar{\xi}$ and $\underline{\xi}(t)$ are covariance matrices for $\bar{\rho}$ and $\underline{\rho}$, respectively. $\bar{\chi}(t)$ and $\underline{\chi}(t)$ are

$$\begin{aligned}\bar{\chi} &= [\bar{\chi}_1, \dots, \bar{\chi}_l, \dots, \bar{\chi}_{n_r}]^T, \\ \underline{\chi} &= [\underline{\chi}_1, \dots, \underline{\chi}_l, \dots, \underline{\chi}_{n_r}]^T,\end{aligned}\quad (16)$$

where $\bar{\chi}_l$ and $\underline{\chi}_l$ are

$$\begin{aligned}\bar{\chi}_l &= \frac{\partial \hat{y}}{\partial \bar{\rho}_l} = \frac{\partial \hat{y}}{\partial \bar{y}} \frac{\partial \bar{y}}{\partial \bar{\rho}_l} = \frac{\partial \hat{y}}{\partial \bar{y}} \frac{\partial \bar{y}}{\partial \bar{y}_{\beta_h}} \frac{\partial \bar{y}_{\beta_h}}{\partial \bar{\rho}_l} + \frac{\partial \hat{y}}{\partial \bar{y}} \frac{\partial \bar{y}}{\partial \bar{y}_{\beta_h}} \frac{\partial \bar{y}_{\beta_h}}{\partial \bar{\rho}_l} \\ &= 0.5 \frac{1}{\sum_{h=1}^n (\bar{\beta}_h + \underline{\beta}_h)} \sum_{h=1}^n \bar{\beta}_h \frac{\bar{\eta}_{\beta_h}^l}{\sum_{l=1}^{n_r} (\bar{\eta}_{\beta_h}^l + \underline{\eta}_{\beta_h}^l)} +\end{aligned}$$

$$= 0.5 \frac{1}{\sum_{h=1}^n (\bar{\beta}_h + \underline{\beta}_h)} \sum_{h=1}^n \underline{\beta}_h \frac{\bar{\eta}_{\beta_h}^l}{\sum_{l=1}^{n_r} (\bar{\eta}_{\beta_h}^l + \underline{\eta}_{\beta_h}^l)},$$

$$\underline{\chi}_l = \frac{\partial \hat{y}}{\partial \underline{\rho}_l} = \frac{\partial \hat{y}}{\partial \bar{y}} \frac{\partial \bar{y}}{\partial \underline{\rho}_l} = \frac{\partial \hat{y}}{\partial \bar{y}} \frac{\partial \bar{y}}{\partial \bar{y}_{\beta_h}} \frac{\partial \bar{y}_{\beta_h}}{\partial \underline{\rho}_l} + \frac{\partial \hat{y}}{\partial \bar{y}} \frac{\partial \bar{y}}{\partial \bar{y}_{\beta_h}} \frac{\partial \bar{y}_{\beta_h}}{\partial \underline{\rho}_l}$$

$$= 0.5 \frac{1}{\sum_{h=1}^n (\bar{\beta}_h + \underline{\beta}_h)} \sum_{h=1}^n \bar{\beta}_h \frac{\underline{\eta}_{\beta_h}^l}{\sum_{l=1}^{n_r} (\bar{\eta}_{\beta_h}^l + \underline{\eta}_{\beta_h}^l)} +$$

$$= 0.5 \frac{1}{\sum_{h=1}^n (\bar{\beta}_h + \underline{\beta}_h)} \sum_{h=1}^n \underline{\beta}_h \frac{\underline{\eta}_{\beta_h}^l}{\sum_{l=1}^{n_r} (\bar{\eta}_{\beta_h}^l + \underline{\eta}_{\beta_h}^l)}.$$

(17)

8.2. *Tuning of MF Parameters.* The centers of MFs are adjusted using the gradient descent. The tuning laws are therefore written as follows:

$$c_{M_c^j}(t) = c_{M_c^j}(t-1) - \gamma \frac{\partial J}{\partial c_{M_c^j}}, \quad j = 1, 2,$$

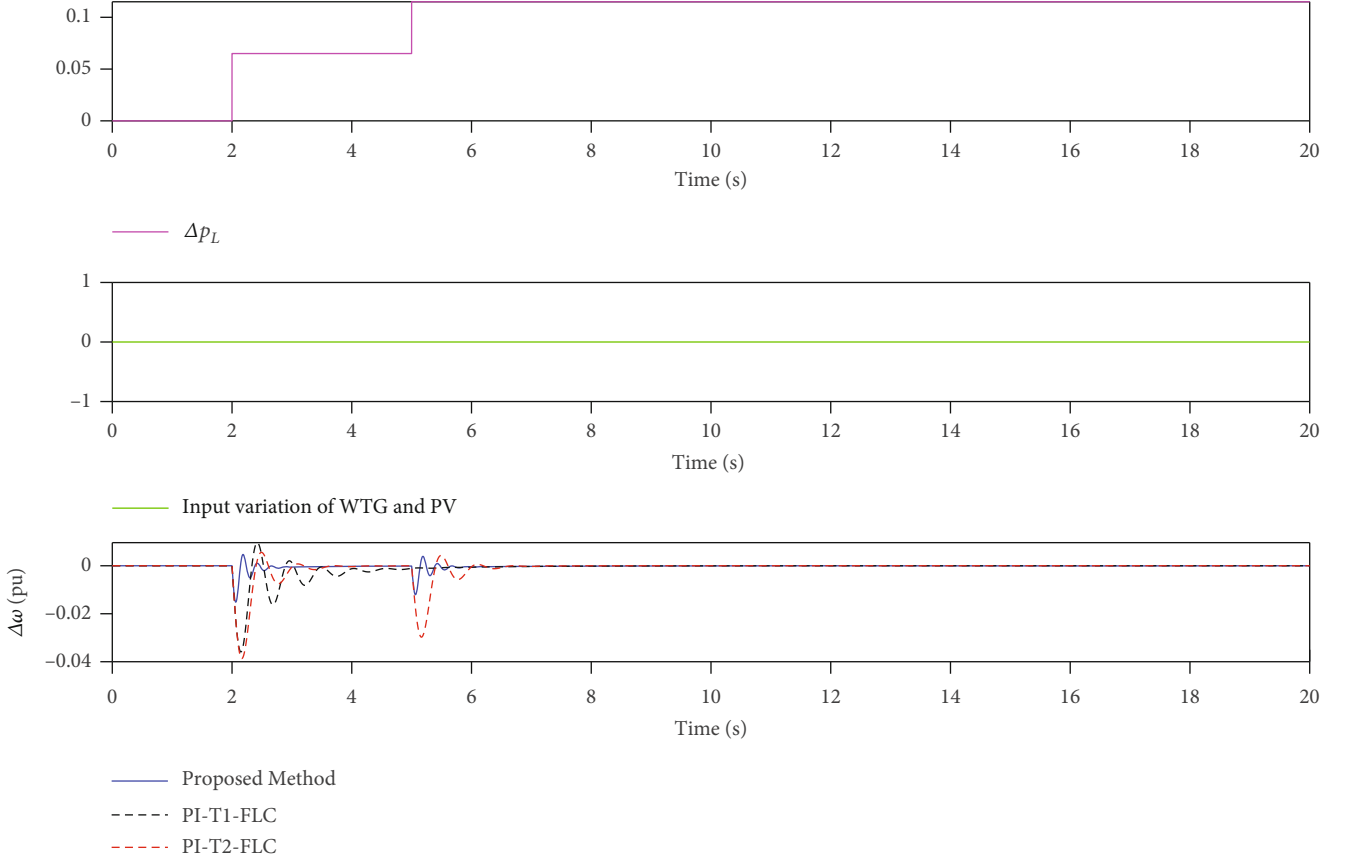


FIGURE 8: Scenario 2: multiple load changes.

$$c_{\bar{M}_{I_e}^j} (t) = c_{\bar{M}_{I_e}^j} (t-1) - \gamma \frac{\partial J}{\partial c_{\bar{M}_{I_e}^j}}, j = 1, 2,$$

$$c_{\bar{M}_{D_e}^j} (t) = c_{\bar{M}_{D_e}^j} (t-1) - \gamma \frac{\partial J}{\partial c_{\bar{M}_{D_e}^j}}, j = 1, 2,$$
(18)

where γ is a constant rate. $\partial J / \partial c_{\bar{M}_e^1}$ is

$$\begin{aligned} \frac{\partial J}{\partial c_{\bar{M}_e^1}} &= \frac{\partial J}{\partial \bar{y}} \frac{\partial \bar{y}}{\partial \bar{y}} \frac{\partial \bar{y}}{\partial \bar{y}_{\beta_h}} \left(\sum_{l=1}^{n_r} \bar{c}_e^l \frac{\partial \bar{y}_{\beta_h}}{\partial \bar{\eta}_{\beta_h}^l} \frac{\partial \bar{\eta}_{\beta_h}^l}{\partial c_{\bar{M}_e^1}} + \sum_{l=1}^{n_r} \bar{c}_e^l \frac{\partial \bar{y}_{\beta_h}}{\partial \bar{\eta}_{\beta_h}^l} \frac{\partial \eta_{\beta_h}^l}{\partial c_{\bar{M}_e^1}} \right) + \\ &= \frac{\partial J}{\partial \bar{y}} \frac{\partial \bar{y}}{\partial \bar{y}} \frac{\partial \bar{y}}{\partial \bar{y}_{\beta_h}} \left(\sum_{l=1}^{n_r} \bar{c}_e^l \frac{\partial \bar{y}_{\beta_h}}{\partial \bar{\eta}_{\beta_h}^l} \frac{\partial \bar{\eta}_{\beta_h}^l}{\partial c_{\bar{M}_e^1}} + \sum_{l=1}^{n_r} \bar{c}_e^l \frac{\partial \bar{y}_{\beta_h}}{\partial \bar{\eta}_{\beta_h}^l} \frac{\partial \eta_{\beta_h}^l}{\partial c_{\bar{M}_e^1}} \right) + \\ &= \frac{\partial J}{\partial \bar{y}} \frac{\partial \bar{y}}{\partial \bar{y}} \frac{\partial \bar{y}}{\partial \bar{y}_{\beta_h}} \left(\sum_{l=1}^{n_r} \bar{c}_e^l \frac{\partial \bar{y}_{\beta_h}}{\partial \bar{\eta}_{\beta_h}^l} \frac{\partial \bar{\eta}_{\beta_h}^l}{\partial c_{\bar{M}_e^1}} + \sum_{l=1}^{n_r} \bar{c}_e^l \frac{\partial \bar{y}_{\beta_h}}{\partial \bar{\eta}_{\beta_h}^l} \frac{\partial \eta_{\beta_h}^l}{\partial c_{\bar{M}_e^1}} \right) + \\ &= \frac{\partial J}{\partial \bar{y}} \frac{\partial \bar{y}}{\partial \bar{y}} \frac{\partial \bar{y}}{\partial \bar{y}_{\beta_h}} \left(\sum_{l=1}^{n_r} \bar{c}_e^l \frac{\partial \bar{y}_{\beta_h}}{\partial \bar{\eta}_{\beta_h}^l} \frac{\partial \bar{\eta}_{\beta_h}^l}{\partial c_{\bar{M}_e^1}} + \sum_{l=1}^{n_r} \bar{c}_e^l \frac{\partial \bar{y}_{\beta_h}}{\partial \bar{\eta}_{\beta_h}^l} \frac{\partial \eta_{\beta_h}^l}{\partial c_{\bar{M}_e^1}} \right), \end{aligned}$$
(19)

where \bar{c}_e^l denotes the l th element of \bar{c}_e . \bar{c}_e is written as

$$\bar{c}_e = [1, 1, 1, 1, 0, 0, 0, 0], \quad (20)$$

where the components of \bar{c}_e in rules that contain $c_{\bar{M}_e^1}$ are one.

$\frac{\partial \bar{y}_{\beta_h}}{\partial \bar{\eta}_{\beta_h}^l}, \frac{\partial \bar{y}_{\beta_h}}{\partial \bar{\eta}_{\beta_h}^l}$ are written as

$$\begin{aligned} \frac{\partial \bar{y}_{\beta_h}}{\partial \bar{\eta}_{\beta_h}^l} &= \bar{\rho}_l \frac{\sum_{l=1}^{n_r} (\bar{\eta}_{\beta_h}^l + \eta_{\beta_h}^l) - \bar{\eta}_{\beta_h}^l}{\left(\sum_{l=1}^{n_r} (\bar{\eta}_{\beta_h}^l + \eta_{\beta_h}^l) \right)^2}, \\ \frac{\partial \bar{y}_{\beta_h}}{\partial \eta_{\beta_h}^l} &= \bar{\rho}_l \frac{-1}{\left(\sum_{l=1}^{n_r} (\bar{\eta}_{\beta_h}^l + \eta_{\beta_h}^l) \right)^2}, \\ \frac{\partial \bar{y}_{\beta_h}}{\partial \bar{\eta}_{\beta_h}^l} &= \bar{\rho}_l \frac{\sum_{l=1}^{n_r} (\bar{\eta}_{\beta_h}^l + \eta_{\beta_h}^l) - \bar{\eta}_{\beta_h}^l}{\left(\sum_{l=1}^{n_r} (\bar{\eta}_{\beta_h}^l + \eta_{\beta_h}^l) \right)^2}, \\ \frac{\partial \bar{y}_{\beta_h}}{\partial \eta_{\beta_h}^l} &= \bar{\rho}_l \frac{-1}{\left(\sum_{l=1}^{n_r} (\bar{\eta}_{\beta_h}^l + \eta_{\beta_h}^l) \right)^2}, \end{aligned}$$

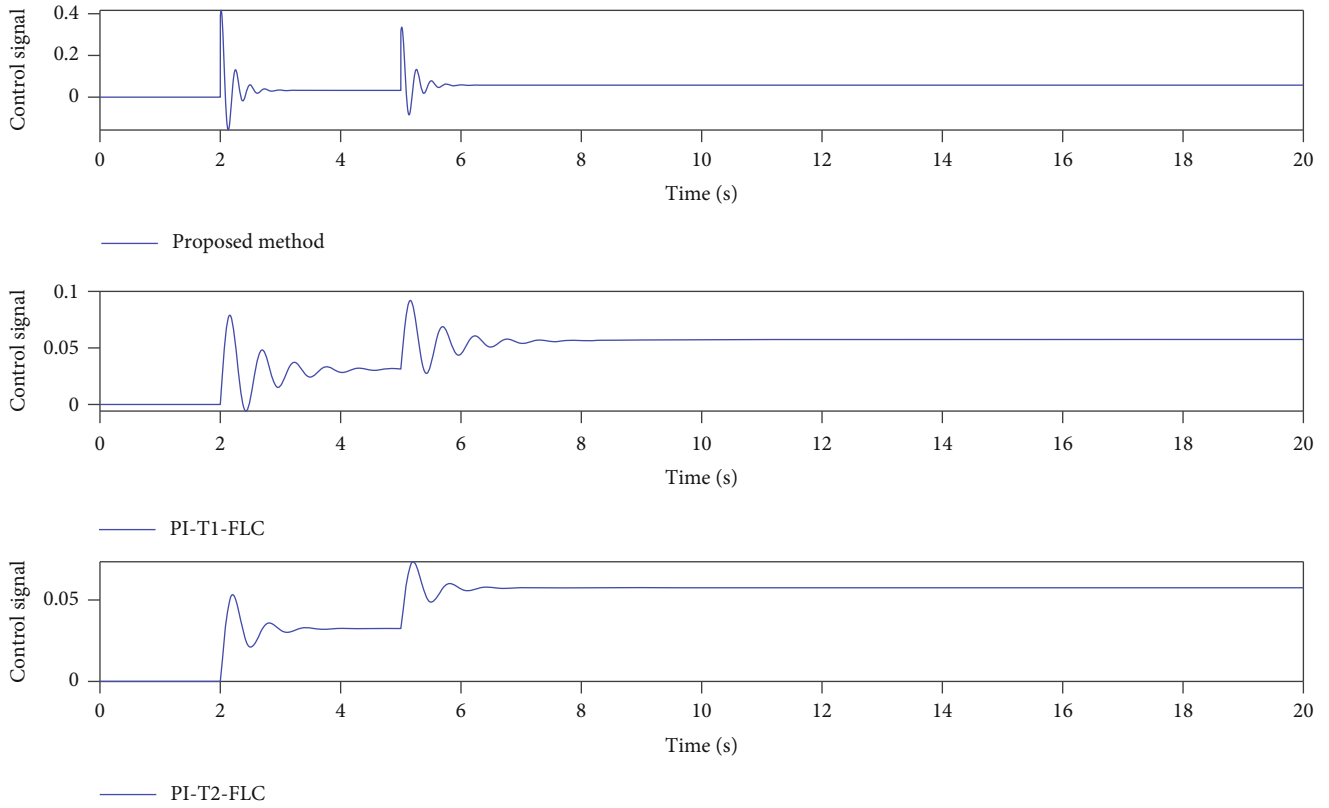


FIGURE 9: Scenario 2: control signals.

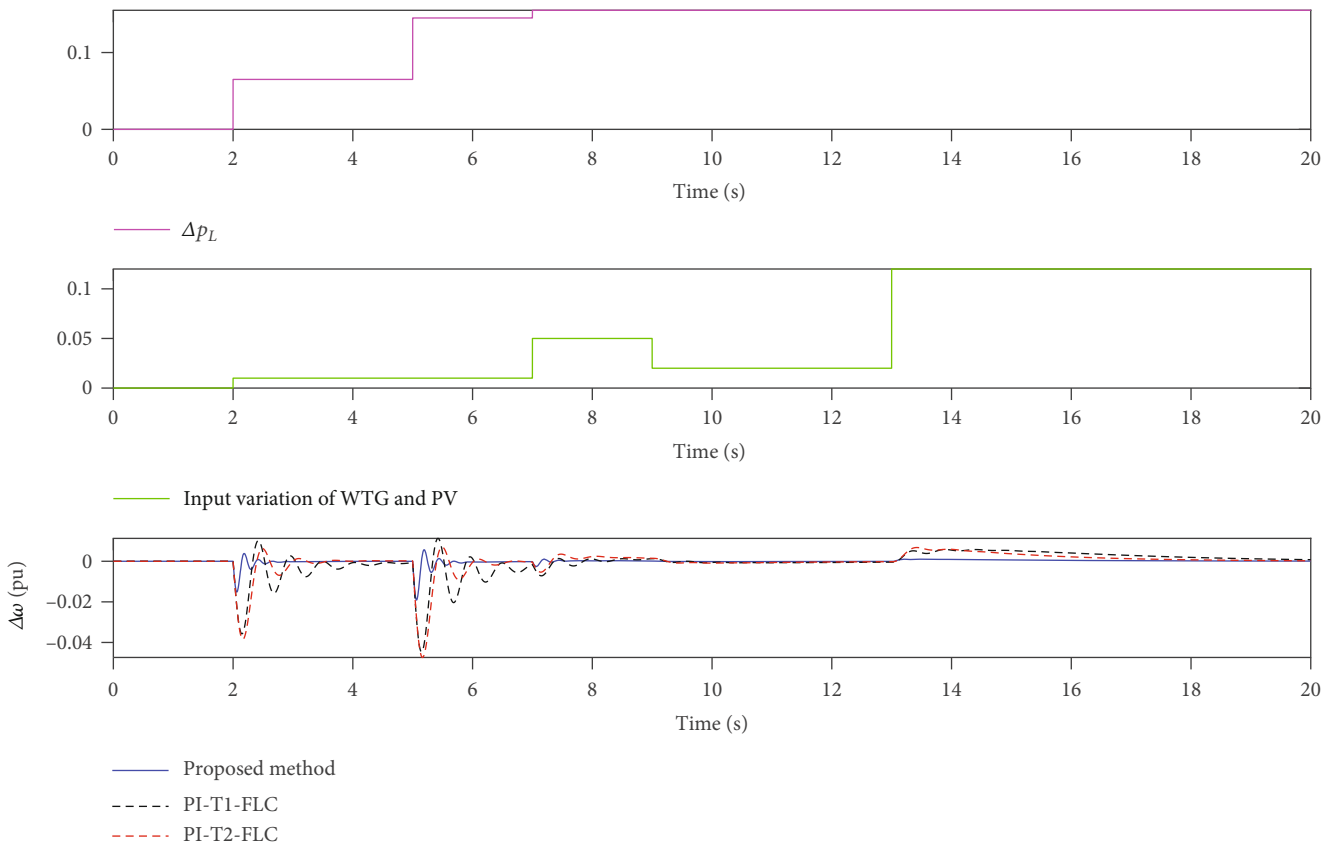


FIGURE 10: Scenario 3: multiple changes in load and irradiation wind power.

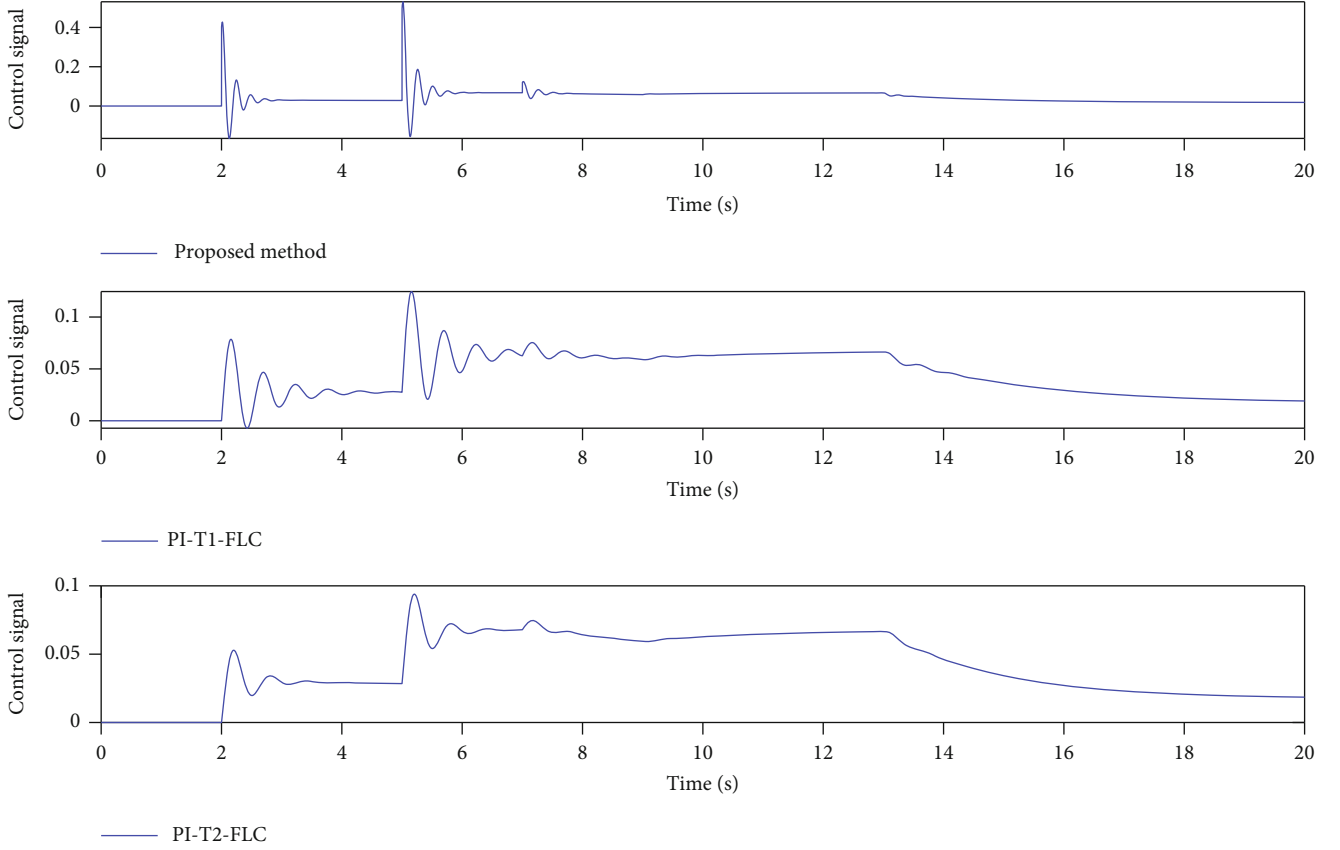


FIGURE 11: Scenario 3: control signals.

TABLE 2: RMSE comparison.

Scenarios	Designed controller	PI-T1-FLC [41]	PI-T2-FLC [42]	GT2-FLC [29]
	0.0012	0.0124	0.0106	0.0052
	0.0014	0.0065	0.0062	0.0035
	0.0016	0.0079	0.0074	0.0018

$$\frac{\partial \hat{y}_{\beta_h}}{\partial \bar{\eta}_{\beta_h}^l} = \rho_l \frac{\sum_{l=1}^{n_r} (\bar{\eta}_{\beta_h}^l + \underline{\eta}_{\beta_h}^l) - \bar{\eta}_{\beta_h}^l}{\left(\sum_{l=1}^{n_r} (\bar{\eta}_{\beta_h}^l + \underline{\eta}_{\beta_h}^l) \right)^2},$$

$$\frac{\partial \hat{y}_{\beta_h}}{\partial \underline{\eta}_{\beta_h}^l} = \rho_l \frac{-1}{\left(\sum_{l=1}^{n_r} (\bar{\eta}_{\beta_h}^l + \underline{\eta}_{\beta_h}^l) \right)^2},$$

$$\frac{\partial \hat{y}_{\beta_h}}{\partial \bar{\eta}_{\beta_h}^l} = \rho_l \frac{\sum_{l=1}^{n_r} (\bar{\eta}_{\beta_h}^l + \underline{\eta}_{\beta_h}^l) - \bar{\eta}_{\beta_h}^l}{\left(\sum_{l=1}^{n_r} (\bar{\eta}_{\beta_h}^l + \underline{\eta}_{\beta_h}^l) \right)^2},$$

$$\frac{\partial \hat{y}_{\beta_h}}{\partial \underline{\eta}_{\beta_h}^l} = \rho_l \frac{-1}{\left(\sum_{l=1}^{n_r} (\bar{\eta}_{\beta_h}^l + \underline{\eta}_{\beta_h}^l) \right)^2}.$$

(21)

For $\partial \bar{\eta}_{\beta_h}^l / \partial c_{\bar{M}_e^1}$, $\partial \bar{\eta}_{\beta_h}^l / \partial c_{\bar{M}_e^1}$, $\partial \eta_{\beta_h}^l / \partial c_{\bar{M}_e^1}$, and $\partial \eta_{\beta_h}^l / \partial c_{\bar{M}_e^1}$, one has

$$\begin{aligned} \frac{\partial \bar{\eta}_{\beta_h}^l}{\partial c_{\bar{M}_e^1}} &= \frac{2(e - c_{\bar{M}_e^1 | \beta_h})}{\bar{\vartheta}_{\bar{M}_e^1 | \beta_h}^2} \bar{\eta}_{\beta_h}^l, \\ \frac{\partial \bar{\eta}_{\beta_h}^l}{\partial c_{\bar{M}_e^1}} &= \frac{2(e - c_{\bar{M}_e^1 | \beta_h})}{\bar{\vartheta}_{\bar{M}_e^1 | \beta_h}^2} \bar{\eta}_{\beta_h}^l, \\ \frac{\partial \eta_{\beta_h}^l}{\partial c_{\bar{M}_e^1}} &= \frac{2(e - c_{\bar{M}_e^1 | \beta_h})}{\bar{\vartheta}_{\bar{M}_e^1 | \beta_h}^2} \eta_{\beta_h}^l, \\ \frac{\partial \eta_{\beta_h}^l}{\partial c_{\bar{M}_e^1}} &= \frac{2(e - c_{\bar{M}_e^1 | \beta_h})}{\bar{\vartheta}_{\bar{M}_e^1 | \beta_h}^2} \eta_{\beta_h}^l. \end{aligned} \quad (22)$$

The computation of $\partial J / \partial c_{\bar{M}_e^2}$, $\partial J / \partial c_{\bar{M}_e^2}$, $\partial J / \partial c_{\bar{M}_e^2}$, $\partial J / \partial c_{\bar{M}_e^2}$, and $\partial J / \partial c_{\bar{M}_e^2}$ are the same as $\partial J / \partial c_{\bar{M}_e^1}$, with just difference that \bar{c}_e is replaced with \underline{c}_e , $\bar{c}_{D_e^1}$, $\underline{c}_{D_e^1}$, $\bar{c}_{I_e^1}$, and $\underline{c}_{I_e^1}$, respectively. Also, $c_{\bar{M}_e^1 | \beta_h}$, $c_{\bar{M}_e^1 | \beta_h}$, $\bar{\vartheta}_{\bar{M}_e^1 | \beta_h}$, and $\bar{\vartheta}_{\bar{M}_e^1 | \beta_h}$ must be

replaced with the corresponding terms. The vectors $\underline{\zeta}_e$, $\bar{\zeta}_{D_i^q e}$, $\underline{\zeta}_{D_i^q e}$, $\bar{\zeta}_{I_i^q e}$, and $\underline{\zeta}_{I_i^q e}$ are as

$$\begin{aligned}\underline{\zeta}_e &= [0, 0, 0, 0, 1, 1, 1, 1], \\ \bar{\zeta}_{D_i^q e} &= [1, 0, 1, 0, 1, 0, 1, 0], \\ \underline{\zeta}_{D_i^q e} &= [0, 1, 0, 1, 0, 1, 0, 1], \\ \bar{\zeta}_{I_i^q e} &= [1, 1, 0, 0, 1, 1, 0, 0], \\ \underline{\zeta}_{I_i^q e} &= [0, 0, 1, 1, 0, 0, 1, 1].\end{aligned}\quad (23)$$

9. Simulations

The designed controller is applied on a case-study MG that is shown in Figure 5 [29] and is described in Table 1 [29]. Time-varying dynamics, rapid power changes and solar irradiation, multiple load changes, and so on are all considered in the evaluation of the LFC's regulatory performance.

Scenario 1: a single load perturbation is taken into account in the initial set of parameters. Also, the model information of all units is unknown. Figure 6 shows the regulation performance. Figure 7 shows the controller signal. Comparison with type-1 fuzzy controller (PI-T1-FLC) [41] and type-2 FLC (PI-T2-FLC) [42] shows that the suggested approach is superior in terms of overall performance and accuracy. An observer can clearly tell that the designed control system is able to outperform.

Scenario 2: in addition to the perturbation of previous scenario, in the second case, the values of all unit parameters are considered to be time-varying as $p = (1 + \cos(t))p$. Figure 8 depicts the system's regulation outcome. Figure 9 show the controller signal. It is clear from Figure 8 that the proposed FLC performs exceptionally well.

Scenario 3: the solar/wind powers are also time-varying in the third scenario, in addition to the numerous fluctuations in the load. Also, a sensor error is added to output signals as a Gaussian noise with variance 0.01. Figure 10 shows the frequency's performance in this situation. Figure 11 shows the controller signal. One can see that the proposed technique holds up well in the face of solar variation, wind turbine mechanical power disturbance, and various load variations. In comparison to the other controllers, the suggested method's frequency trajectory shows less variance. Table 2 contains the RMSE values for each of the various cases. The performance is compared with PI-T1-FLC [41], PI-T2-FLC [42], and general type-2 FLC (GT2-FLC) [29]. The suggested method's RMSE in all circumstances appear to be significantly lower than those of the other techniques.

10. Conclusion

The applications of renewable energies (REs) in meeting the energy needs of human societies are extended, because the use of RE sources can prevent the emission of greenhouse gases and pollutants, reduce water consumption, and ultimately help sustainable security. One of the main drawbacks is the natural fluctuation of voltage/frequency in microgrids (MGs) that include RE sources. In this paper, a new scheme

is developed for frequency management in MGs. A new T3-FLS-based controller is designed, and an online optimization scheme is proposed. The designed controller is applied for an MG, and its performance is evaluated under various practical conditions. In the first scenario, in addition to unknown dynamics, an abrupt change is considered in the output load. It is shown that the suggested controller well handles the disturbances, and the output is stabilized in a finite time. For the second examination, another is added to the previous one, and the parameters of the MG dynamics are considered to be time-varying. The simulation results are verified that the suggested approach well resists against dynamic perturbations. Finally, for the last examination, beside the dynamic uncertainties and load perturbations, the solar/wind powers are also changed, and a sensor error is added to signals as a Gaussian noise with variance 0.01. The results and comparisons with other approaches demonstrate that the suggested controller has a good regulation outcome with the least steady-state error and good transient performance.

Nomenclature

FLSs:	Fuzzy logic systems
PI:	Proportional-integral
T3:	Type 3
MG:	Microgrid
RE:	Renewable energies
GA:	Genetic algorithm
PSO:	Particle swarm optimization
LFC:	Load frequency control
MF:	Membership function
SD:	Standard divisions
FLC:	Fuzzy controller.

Data Availability

All the numerical simulation parameters are mentioned in the respective text part, and there are no additional data requirements for the simulation results.

Conflicts of Interest

The authors declare that there is no conflict of interest.

References

- [1] A. H. T. Yabr, S. E. Najafi, Z. Moghaddas, and P. S. Shahrezaei, "Interval cross efficiency measurement for general two-stage systems," *Mathematical Problems in Engineering*, vol. 2022, Article ID 5431358, 19 pages, 2022.
- [2] T. Xiao, C. Gan, and Q. Zhang, "The existence of least energy sign-changing solution for Kirchhoff-type problem with potential vanishing at infinity," *Advances in Mathematical Physics*, vol. 2021, Article ID 6690204, 10 pages, 2021.
- [3] H.-A. Trinh, H.-V.-A. Truong, and K. K. Ahn, "Development of fuzzy-adaptive control based energy management strategy for PEM fuel cell hybrid tramway system," *Applied Sciences*, vol. 12, no. 8, p. 3880, 2022.
- [4] H. V. A. Truong, H. A. Trinh, D. T. Tran, and K. K. Ahn, "A robust observer for sensor faults estimation on n-DOF

- manipulator in constrained framework environment," *IEEE Access*, vol. 9, pp. 88439–88451, 2021.
- [5] C. Zhu, Q. Tu, C. Jiang, M. Pan, H. Huang, and Z. Tu, "Mean deviation coupling control for multimotor system via global fast terminal sliding mode control," *Advances in Mathematical Physics*, vol. 2021, Article ID 9200267, 16 pages, 2021.
- [6] H. Salahuddin, K. Imdad, M. U. Chaudhry, D. Nazarenko, V. Bolshev, and M. Yasir, "Induction machine-based EV vector control model using Mamdani fuzzy logic controller," *Applied Sciences*, vol. 12, no. 9, p. 4647, 2022.
- [7] R. Ashraf, M. A. Habib, M. Akram et al., "Deep convolution neural network for big data medical image classification," *IEEE Access*, vol. 8, pp. 105659–105670, 2020.
- [8] A. Tabak, "Fractional order frequency proportional-integral-derivative control of microgrid consisting of renewable energy sources based on multi-objective grasshopper optimization algorithm," *Transactions of the Institute of Measurement and Control*, vol. 44, no. 2, pp. 378–392, 2022.
- [9] R. Tripathi and O. Singh, "An analysis on frequency control of microgrid including diverse renewable energy sources," in *Advances in Energy Technology*, pp. 81–95, Springer, 2022.
- [10] H. M. El Zoghby and H. S. Ramadan, "Isolated microgrid stability reinforcement using optimally controlled STATCOM," *Sustainable Energy Technologies and Assessments*, vol. 50, article 101883, 2022.
- [11] G. K. Suman, J. M. Guerrero, and O. P. Roy, "Stability of microgrid cluster with diverse energy sources: a multi-objective solution using NSGA-II based controller," *Sustainable Energy Technologies and Assessments*, vol. 50, article 101834, 2022.
- [12] K. A. Al Sumarmad, N. Sulaiman, N. I. A. Wahab, and H. Hizam, "Energy management and voltage control in microgrids using artificial neural networks, PID, and fuzzy logic controllers," *Energies*, vol. 15, no. 1, p. 303, 2022.
- [13] H. K. Vanashi, F. D. Mohammadi, V. Verma, J. Solanki, and S. K. Solanki, "Hierarchical multi-agent based frequency and voltage control for a microgrid power system," *International Journal of Electrical Power & Energy Systems*, vol. 135, article 107535, 2022.
- [14] M. Ranjan and R. Shankar, "A literature survey on load frequency control considering renewable energy integration in power system: recent trends and future prospects," *Journal of Energy Storage*, vol. 45, article 103717, 2022.
- [15] R. Kumar, S. Jha, and R. Singh, "A different approach for solving the shortest path problem under mixed fuzzy environment," *International Journal of Fuzzy System Applications*, vol. 9, no. 2, pp. 132–161, 2020.
- [16] S. Deng, C. Wang, Z. Fu, and M. Wang, "An intelligent system for insider trading identification in Chinese security market," *Computational Economics*, vol. 57, no. 2, pp. 593–616, 2021.
- [17] M. Vilela, G. Oluyemi, and A. Petrovski, "A fuzzy inference system applied to value of information assessment for oil and gas industry," *Decision Making: Applications in Management and Engineering*, vol. 2, no. 2, pp. 1–18, 2019.
- [18] E. K. Zavadskas, V. Gediminas, Z. Turskis, Ž. Stević, and A. Mardani, "Modelling procedure for the selection of steel pipes supplier by applying fuzzy AHP method," *Operational Research in Engineering Sciences: Theory and Applications*, vol. 3, no. 2, pp. 39–53, 2020.
- [19] Q. Bu, J. Cai, Y. Liu et al., "The effect of fuzzy PID temperature control on thermal behavior analysis and kinetics study of biomass microwave pyrolysis," *Journal of Analytical and Applied Pyrolysis*, vol. 158, article 105176, 2021.
- [20] D. Sain and B. Mohan, "Modeling, simulation and experimental realization of a new nonlinear fuzzy PID controller using center of gravity defuzzification," *ISA Transactions*, vol. 110, pp. 319–327, 2021.
- [21] T. A. Mai, T. S. Dang, D. T. Duong, V. C. Le, and S. Banerjee, "A combined backstepping and adaptive fuzzy PID approach for trajectory tracking of autonomous mobile robots," *Journal of the Brazilian Society of Mechanical Sciences and Engineering*, vol. 43, no. 3, pp. 1–13, 2021.
- [22] O. Karahan, "Design of optimal fractional order fuzzy PID controller based on cuckoo search algorithm for core power control in molten salt reactors," *Progress in Nuclear Energy*, vol. 139, article 103868, 2021.
- [23] D. Sain and B. Mohan, "A simple approach to mathematical modelling of integer order and fractional order fuzzy PID controllers using one-dimensional input space and their experimental realization," *Journal of the Franklin Institute*, vol. 358, no. 7, pp. 3726–3756, 2021.
- [24] P. C. Nayak, B. P. Nayak, R. C. Prusty, and S. Panda, "Sunflower optimization based fractional order fuzzy PID controller for frequency regulation of solar-wind integrated power system with hydrogen aqua equalizer-fuel cell unit," *Energy Sources, Part A: Recovery, Utilization, and Environmental Effects*, pp. 1–19, 2021.
- [25] A. Aftab and X. Luan, "A fuzzy-PID series feedback self-tuned adaptive control of reactor power using nonlinear multipoint kinetic model under reference tracking and disturbance rejection," *Annals of Nuclear Energy*, vol. 166, article 108696, 2022.
- [26] Y. Liu, K. Fan, and Q. Ouyang, "Intelligent traction control method based on model predictive fuzzy PID control and online optimization for permanent magnetic maglev trains," *IEEE Access*, vol. 9, pp. 29032–29046, 2021.
- [27] M. G. Gafar, R. A. El-Sehiemy, and S. Sarhan, "A hybrid fuzzy-crow optimizer for unconstrained and constrained engineering design problems," *Human-centric Computing and Information Sciences*, vol. 12, pp. 1–24, 2022.
- [28] G. Sahoo, R. K. Sahu, N. R. Samal, and S. Panda, "Analysis of type-2 fuzzy fractional-order PD-PI controller for frequency stabilisation of the micro-grid system with real-time simulation," *International Journal of Sustainable Energy*, vol. 41, no. 5, pp. 412–433, 2022.
- [29] A. Mohammadzadeh, M. H. Sabzalian, A. Ahmadian, and N. Nabipour, "A dynamic general type-2 fuzzy system with optimized secondary membership for online frequency regulation," *ISA Transactions*, vol. 112, pp. 150–160, 2021.
- [30] R. K. Khadanga, A. Kumar, and S. Panda, "Application of interval type-2 fuzzy PID controller for frequency regulation of ac islanded microgrid using modified equilibrium optimization algorithm," *Arabian Journal for Science and Engineering*, vol. 46, no. 10, pp. 9831–9847, 2021.
- [31] K. Sabahi, M. Tavan, and A. Hajizadeh, "Adaptive type-2 fuzzy PID controller for LFC in AC microgrid," *Soft Computing*, vol. 25, no. 11, pp. 7423–7434, 2021.
- [32] P. Jekan and C. Subramani, "The performance analysis of type-2 fuzzy fractional-order tilt integral derivative controller with enhanced Harris hawks optimization," *Transactions of the Institute of Measurement and Control*, vol. 43, no. 12, pp. 2818–2834, 2021.

- [33] S. Rawat, B. Jha, M. K. Panda, and J. Kanti, "Interval type-2 fuzzy logic control-based frequency control of hybrid power system using DMGS of PI controller," *Applied Sciences*, vol. 11, no. 21, p. 10217, 2021.
- [34] Y. Cao, A. Raise, A. Mohammadzadeh, S. Rathinasamy, S. S. Band, and A. Mosavi, "Deep learned recurrent type-3 fuzzy system: application for renewable energy modeling/prediction," *Energy Reports*, vol. 7, pp. 8115–8127, 2021.
- [35] Z. Liu, A. Mohammadzadeh, H. Turabieh, M. Mafarja, S. S. Band, and A. Mosavi, "A new online learned interval type-3 fuzzy control system for solar energy management systems," *IEEE Access*, vol. 9, pp. 10498–10508, 2021.
- [36] M. Gheisarnejad, A. Mohammadzadeh, H. Farsizadeh, and M.-H. Khooban, "Stabilization of 5G telecom converter-based deep type-3 fuzzy machine learning control for telecom applications," *IEEE Transactions on Circuits and Systems II: Express Briefs*, vol. 69, no. 2, pp. 544–548, 2022.
- [37] M. Gheisarnejad, A. Mohammadzadeh, and M. Khooban, "Model predictive control-based type-3 fuzzy estimator for voltage stabilization of DC power converters," *IEEE Transactions on Industrial Electronics*, vol. 69, no. 12, pp. 13849–13858, 2022.
- [38] M. Li, H. S. Dizaji, S. Asaadi, F. Jarad, A. E. Anqi, and M. Wae-hayee, "Thermo-economic, exergetic and mechanical analysis of thermoelectric generator with hollow leg structure; impact of leg cross-section shape and hollow-to-filled area ratio," *Case Studies in Thermal Engineering*, vol. 27, article 101314, 2021.
- [39] J. Li, J. Geng, and T. Yu, "Grid-area coordinated load frequency control strategy using large-scale multi-agent deep reinforcement learning," *Energy Reports*, vol. 8, pp. 255–274, 2022.
- [40] A. Mohammadzadeh, M. H. Sabzalian, and W. Zhang, "An interval type-3 fuzzy system and a new online fractional-order learning algorithm: theory and practice," *IEEE Transactions on Fuzzy Systems*, vol. 28, no. 9, pp. 1940–1950, 2019.
- [41] M. Mokhtar, M. I. Marei, M. A. Sameh, and M. A. Attia, "An adaptive load frequency control for power systems with renewable energy sources," *Energies*, vol. 15, no. 2, p. 573, 2022.
- [42] A. D. Shakibjoo, M. Moradzadeh, S. U. Din, A. Mohammadzadeh, A. H. Mosavi, and L. Vandeveld, "Optimized type-2 fuzzy frequency control for multi-area power systems," *IEEE Access*, vol. 10, pp. 6989–7002, 2022.